Analog tunable gratings driven by thin-film piezoelectric microelectromechanical actuators

Chee Wei Wong, Yongbae Jeon, George Barbastathis, and Sang-Gook Kim

We present a microfabricated grating whose period can be tuned in analog fashion to within a fraction of a nanometer. The tunable angular range is more than 400 μrad in the first diffracted order. The design concept consists of a diffractive grating defined onto a 400-nm membrane, with the membrane subsequently strained in the direction perpendicular to the grating grooves by thin-film piezoelectric actuation. The strain-tuned grating device was fabricated with microelectromechanical processes, utilizing both surface and bulk micromachining. The fabricated piezoelectric film achieved a measured dielectric constant of 1200. Device characterization yielded grating period changes up to 8.3 nm (0.21% strain in the membrane) at 10 V and a diffracted angular change of 486 μrad, in good agreement with the theory. Uniformity across the actuated grating and out-of-plane deflections are characterized and discussed.

OCIS codes: 050.1950, 010.1080, 160.2260, 230.3990.

1. Introduction

Optical microelectromechanical devices have included micromirrors for beam steering in projection displays and optical cross connects, tunable Fabry–Perot cavities for variable-wavelength vertical-cavity surface-emitting lasers, and gratings with tunable dispersion, among many others. We refer to state-of-the-art tunable gratings as digital: for example, the grating light valve,[1] the polychromator,[2] or liquid-crystal phased arrays with addressable electrodes for beam steering.[3] The grating light valve design consists of suspended mechanical beams that form the optical grating. When the beams are unactuated, all beams are at the same height and the device acts optically as a mirror. Electrostatic actuation lowers sets of alternating beams, thus forming gratings of arbitrary periods. The polychromator acts on a similar optical principle, although the beams are individually actuated; hence diffractive optical elements more general than gratings can be implemented. The minimum grating period change that can be achieved in either of these digital devices, and hence the resolution of the tunable grating, is set by the size of each grating beam (typically 1–5 μm).

Analog tunability on diffractive gratings has been reported by use of several mechanisms. Thermally actuated gratings demonstrate diffraction-angle modulation from 1 to 35 mrad.[4,5] Other actuators include (1) motion of a seismic mass to strain a fiber Bragg grating in a planar waveguide[6]; (2) acoustic modulation to scan the transmitted optical beam angle[7]; (3) electrostatic actuation for vertical deflection of the whole grating structure to modulate the diffracted-order intensities, although the diffracted angles are unvaried[4]; and (4) electrostatic actuation for variable blaze gratings, with reported deflection up to 44 mrad.[8]

In this paper we propose a method of analog spatial modulation to achieve tunability in the diffracted angle by up to 400 μrad, with a resolution of the order of 2 μrad. Compared with the digital designs, our device concept trades a smaller deflection range for better angular resolution. Applications for high-resolution analog tunable gratings include external-cavity tunable lasers, thermal compensators and channel monitors for dense wavelength division multiplexing optical networks, and microspectrometers.[9] In our design, the diffraction grating period is tuned in an analog fashion by transverse (in-plane and perpendicular to the grating grooves axis) actuation forces applied on the grating structure. This is illustrated in Fig. 1, where the grating period is pro-

The authors are with the Department of Mechanical Engineering, Massachusetts Institute of Technology, Room 5-026,77 Massachusetts Avenue, Cambridge, Massachusetts 02139. C. W. Wong's e-mail address is cheewei@mit.edu.

Received 27 June 2002; revised manuscript received 6 November 2001.

0003-6935/03/040621-06$15.00/0

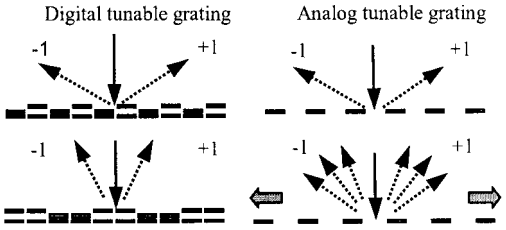

Fig. 1. Actuation concept of analog and digital tunable gratings. The analog design permits analog control of the diffraction angle.

gressively increased, resulting in steering of the diffracted orders.

2. Concepts and Design

To achieve transverse actuation, we first define the grating grooves on a supporting deformable membrane. The membrane is then mechanically strained by thin-film piezoelectric actuators as shown in Fig. 2. The piezoelectric actuators, a lead zirconate titanate oxide (PZT) located at the ends of the membrane, are capable of producing sufficient force to strain the membrane up to an order of 0.3%, or equivalently, 0.3% diffracted-angle change. This is accomplished through application of an electric field across the PZT film to effect its shrinkage, which is due to reorientation of crystallographic domains. This shrinkage on the film correspondingly strains the membrane in the transverse direction and hence the 4-μm period of the superimposed binary-phase grating. Simple in design, this double-hinged membrane configuration, illustrated in Fig. 2, minimizes out-of-plane displacements of the grating grooves from unbalanced film residual stresses and from bending (of a plate with one free end) under actuation. An alternative method of transverse tuning of the grating period involves use of electrostatic comb drives on a more compliant grating structure.[10]

The membrane in-plane displacement modeling, along the grating period axis, begins with a piezoelectric bimorph model where the deformation δ_x is expressed as[11]

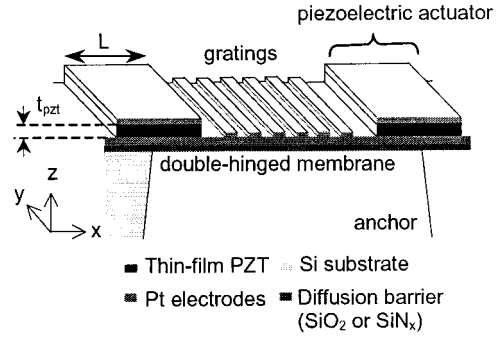

Fig. 2. Design schematic of a double-hinged deformable membrane driven by thin-film piezoelectric actuators. The gratings, defined on top of the membrane, are tuned progressively along with the membrane.

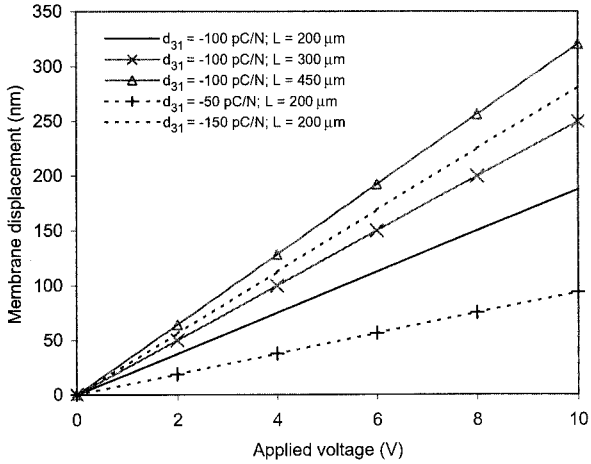

Fig. 3. Calculated grating period change versus applied voltage for various design parameters.

$$\delta_x = \frac{d_{31} E_{\mathrm{PZT}} A V_a}{t_{\mathrm{PZT}} k_x}, \tag{1}$$

where d_{31} is the piezoelectric coupling coefficient, E_i is the ith material Young's modulus, A_i is the ith cross-sectional area, V_a is the applied voltage, t_{PZT} is the thickness of the PZT layer, L is the beam length along the x axis, and k_x is the effective axial stiffness that equals $\Sigma_i E_i A_i / L_i$. Boundary conditions are applied to reflect the double-hinged membrane structure (with symmetry across the membrane midpoint), and the solution is reached iteratively. We note for an isotropic wide membrane,[12] $E_i \rightarrow E_i/(1 - \upsilon_i^2)$ and $d_{31} \rightarrow d_{31}(1 + \upsilon_i)$, where υ is the material Poisson's ratio. Figure 3 shows the period change in an actuated membrane for various design parameters, a linear response that is due to the small displacement. For our double-hinged membrane design parameters ($d_{31} = -100$ pC/N, $E_{\mathrm{PZT}} = 90$ GPa, $t_{\mathrm{PZT}} = 0.5$ μm, and $L = 200$ μm), our analytical model predicts a 187-nm x-axis membrane displacement with a single actuator at 10 V applied and suggests a 5.28-nm grating period change (0.13% membrane strain), assuming uniformity across the membrane. In the small-angle limit, the diffracted angular change $\Delta\theta$ is related to the grating period change as

$$\Delta\theta \cong \frac{m\lambda\Delta d}{d^2}, \tag{2}$$

where m is the diffracted order, λ is the wavelength, Δd is the grating period change, and d is the grating period. For a 632.8-nm laser on a 4-μm grating period, a 5.28-nm period change corresponds to an angular change of 209 μrad for the first diffracted order. On the basis of the fine voltage control[13] previously demonstrated on a thin-film piezoelectric material, the resolution of the grating period change can be

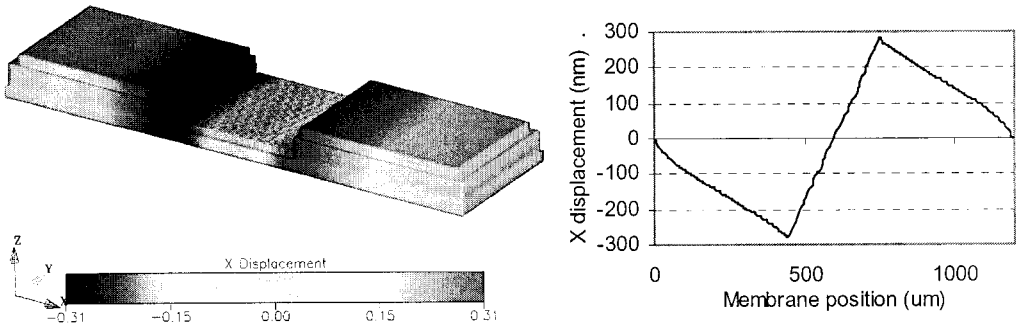

Fig. 4. Finite-element solution of the device design under 10-V actuation to illustrate the x-axis membrane displacement. The z axis is exaggerated 20 times to show the different layers in the membrane. The units shown are in micrometers.

better than 0.5 Å (corresponding to an angular resolution better than 2.1 μrad), although the current metrology limits the observable resolution of the order of 1 nm. Out-of-plane membrane tilt and bending, asymmetrical rotation of the membrane when actuated, thermal disturbances, modal vibrations, and optical detection techniques will limit the achievable resolution.

We used a numerical finite-element tool (CoventorWare) as a comparison with our analytical results. The models are in good agreement—a 280-nm transverse (x-axis) displacement (for $L = 450$ μm) is predicted in the finite-element model, as shown in Fig. 4. The finite-element model predicts a maximum y-axis Poisson contraction of 83 nm across the 300-μm grating and a maximum Mises stress concentration of 220 MPa. In addition, the finite-element model provides an estimate of the membrane out-of-plane bow when actuated. The calculated maximum vertical deflection is 1.941 μm at the center of a 232-μm-long membrane for an applied voltage of 10 V. The bow-shape profile of the actuated grating is added as a nonuniform phase at the object plane with a finite-aperture window. At the Fourier plane, this is observed as a spatial spreading out of the first-diffracted-order energy, although the first-order diffraction efficiency remains approximately unvaried at 20.3%. This is illustrated in comparison with an optically flat diffraction grating in Fig. 5, wherein both cases are considered in the Fraunhofer regime. The membrane bow contributes approximately an additional 56% shift in the first diffracted order, compared with the same grating period actuation on an ideal flat grating. This additional shift needs to be taken into account in the optical design for specific optical telecommunication devices and microspectrometers.

3. Microfabrication Development

The microfabrication process flow of the analog tunable grating is shown in Fig. 6. It utilizes both surface and bulk micromachining to improve device yield. First, a 200-nm silicon nitride layer is deposited by plasma-enhanced chemical vapor deposition and then patterned to form a hard mask for a later potassium hydroxide backside etch. A 220-nm Pt/Ti layer is then evaporated on the substrate and patterned to create the bottom electrode by lift-off, instead of reactive ion etching, to facilitate the fabrication process repeatability. Solgel PZT is subse-

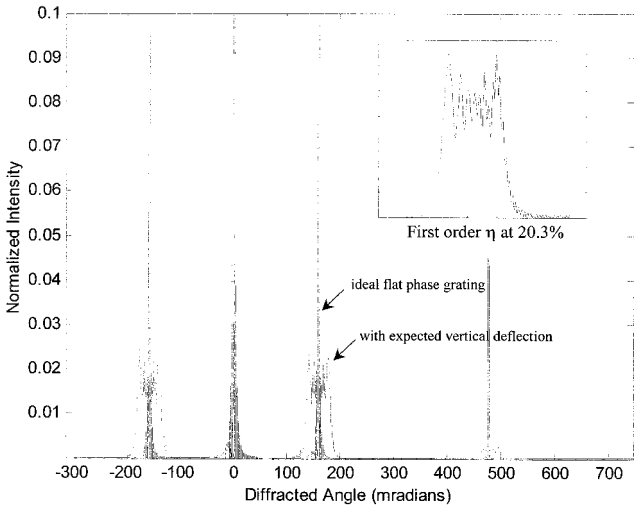

Fig. 5. Intensity profile comparison between an ideal binary-phase grating and one with a bow in the deformable membrane design. The duty cycle and grating step height are taken at 50% and λ/4, respectively, for an ideal grating.

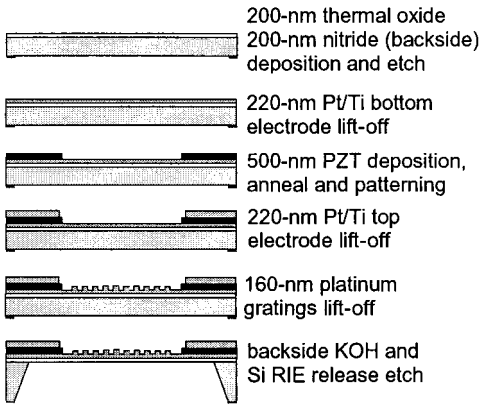

Fig. 6. Microfabrication process flow of the analog tunable grating. The process consists of five masks and involves both surface and bulk micromachining. KOH, potassium hydroxide; RIE, reactive ion etching.

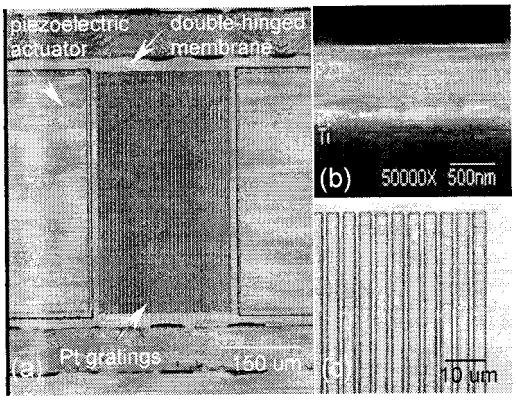

Fig. 7. (a) Piezoelectric-actuated tunable grating under 120× magnification, (b) scanning electron microscopy cross-sectional image of fabricated PZT actuator on Pt/Ti electrodes, (c) magnified view of Pt gratings with a 4-μm period.

quently spun on and annealed in repeated individual steps to create a high-quality PZT layer with 0.5-μm thickness. PZT hillock and crack formation difficulties were resolved with process experimentation of the Pt/Ti bottom electrode and PZT fabrication conditions. The piezoelectric layer is successfully patterned by a rapid wet-etch technique,[14] and the top electrode was deposited with a second 220-nm Pt/Ti evaporation and lift-off procedure. Next, the diffractive grating is separately created with a 160-nm Pt lift-off with 2-μm minimal linewidth features. The double-hinged membrane is then defined with a 445-μm potassium hydroxide backside etch and released with a 5-μm Si reactive ion etching from the backside.

The fabricated device is shown in Fig. 7. The completed PZT has a predominant perovskite phase aided by good adhesion between the bottom Pt/Ti electrode, the SiO_2 diffusion barrier, and the substrate. The average grain size of the PZT film is of the order of 0.1 μm. Ferroelectric characterization

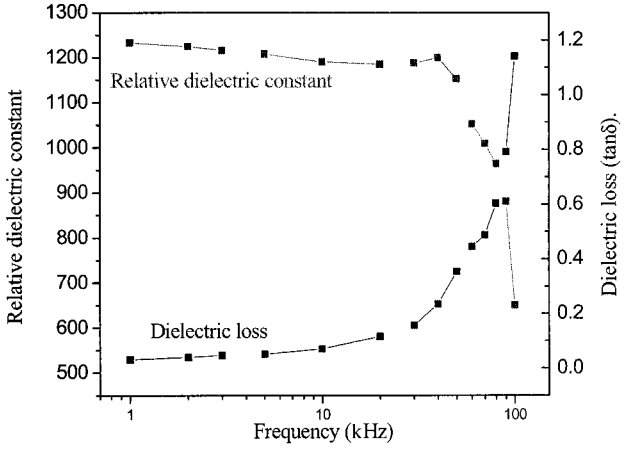

Fig. 8. Ferroelectric response of fabricated PZT film. A relative dielectric constant of 1200 and dielectric loss of less than 0.05 were measured.

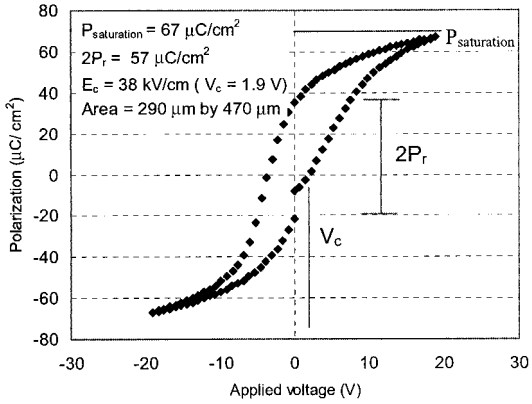

Fig. 9. Hysteresis characterization of piezoelectric film after completion of device fabrication.

(Fig. 8) suggests an excellent dielectric constant of above 1200 and a dielectric loss below 0.05. The coercive field and saturation polarization are estimated at 38 kV/cm and 67 μC/cm^2, respectively, as shown in Fig. 9. Fatigue life-cycle experiments suggest operation above 10^{10} cycles under a 5-V rectangular pulse-train signal. The power consumption of the PZT film at 10-V actuation is gauged at 30 nW, made possible from its high resistivity. The fabricated binary-phase grating also has a measured duty cycle varying between 42% and 66%, depending on the process conditions. First- and third-order diffraction efficiencies were measured at 7.6% and 5.0%, respectively, for the fabricated grating (without actuation), although higher efficiencies could be achieved with better process control.

4. Experimental Results

The membrane deformation by the thin-film PZT actuators is measured with a computer microvision instrument.[15] This instrument reconstructs three-dimensional images of microscopic targets using the optical sectioning property of a light microscope and postprocesses the combined images to analyze the target motion with nanometer precision.

Device 1, which has a 450-μm PZT length, demonstrated a 229 ± 2 nm total membrane displacement at 9 V. From tracking the displacements of the grating beams, we observed an average period change of 8.3 nm (0.21% membrane strain) at 9-V actuation. This corresponds to a theoretical diffracted-angle change of 328 μrad for our fabricated device parameters. Device 2, with a 200-μm PZT length, shows a 4.9-nm period change at 10 V (corresponding to a 0.12% membrane strain and a theoretical 194-μrad diffracted-angle change). The period change at 1 V for both devices is approximately 0.6 nm, calculated from total membrane displacement. As summarized in Fig. 10, both experimental device measurements are in good agreement (correlation coefficient $\rho \sim 0.9$) with the analytical formulation for a single d_{31} coefficient of approximately −100 pC/N. The material properties used in the analytical model are consistent in both plots and fall within the range

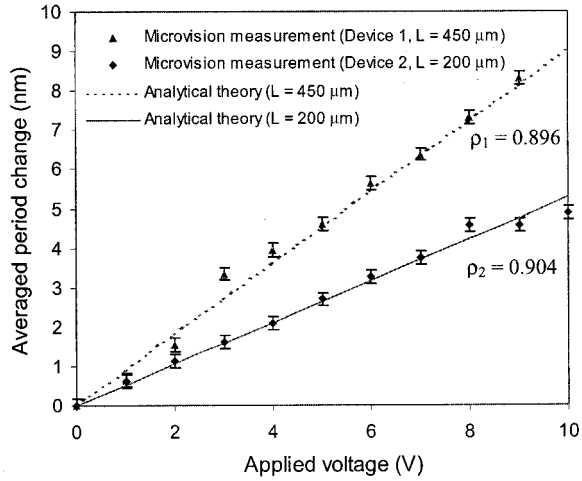

Fig. 10. Measured period change versus applied voltage for two different device designs.[12] Both results match with the analytical model for a single set of material properties and with a single fitted d_{31} coefficient at -100 pC/N.

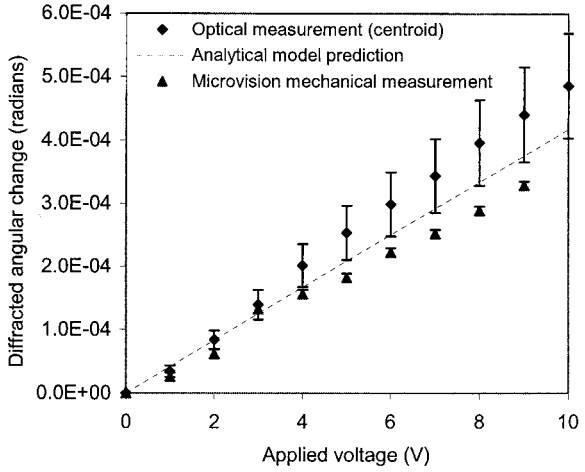

Fig. 12. First-order diffracted angular change versus applied voltage obtained by optical image centroid processing and mechanical motion measurements. The optical measurement is corrected for tilt in the membrane with the finite-element mechanical model and is the main source of uncertainty.

reported in the literature. A direct characterization of the d_{31} coefficient is currently being carried out.

Measurements on strain uniformity, from device 2, are shown in Fig. 11, with the error bars depicting the maximum and minimum values. The average membrane strains (or equivalently, the percentage of the average period change versus the original grating period) for four different regions of the grating are plotted for various applied voltages. An average uniformity percentage of 16%, calculated as the ratio of the standard deviation of the membrane strain to the average membrane strain, is obtained over 40 measurements. The uniformity variation could be due to variation in membrane thickness, especially in the SiO_2 layer after membrane release. This nonuniformity is averaged out in the diffracted orders, although there is a corresponding spatial spreading of the energy in each diffracted order. Therefore, in the design of specific optical systems, the angle of acceptance should be sufficiently large so that the bulk of the diffracted order of interest is captured. The grating grooves also show a measured shrinkage in the lateral (y-axis) direction as expected because of positive strain in the transverse (x-axis) direction.

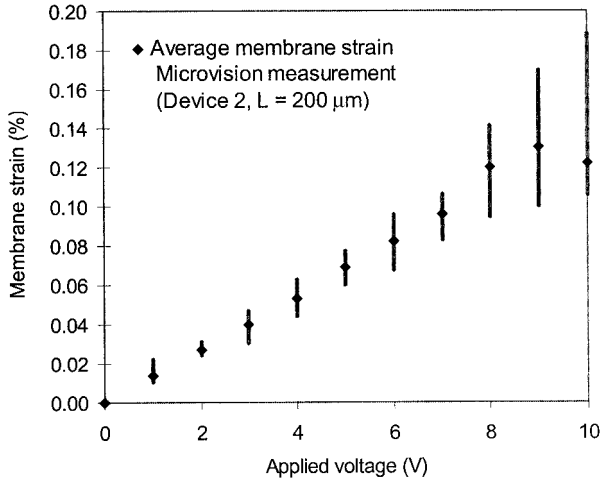

Fig. 11. Uniformity of membrane strain under actuation. A uniformity variation of 16% (defined as the standard deviation over the averaged value) is measured. The error bars depict the maximum and minimum values of the measurements.

The PZT polarization electric field hysteresis behavior, which is due to the domain reorientations, is evident when the membrane is actuated from -10 V to $+10$ V. There is a nonzero membrane displacement at 0 V and a minimum membrane displacement between 2 and 4 V (varies across different devices). This result matches the coercive field from electrical hysteresis characterizations of the PZT film.

We performed the measurement of the diffraction angular change by imaging the first diffracted order onto a CCD camera. A 632.8-nm He–Ne laser was used as the illumination source. The diffracted-order centroid location was computed for various actuated positions. The diffraction angles agree well with diffraction theory. More specifically, Fig. 12 shows the first-diffracted-order angular change when voltage is applied to one of the two device actuators. This angular change is then corrected for tilt in the membrane (by the matched finite-element model described in Section 2) when only one of the two actuators is employed. This result is for a device with the same design parameters as device 1. Comparisons among the optical image centroid processing, mechanical membrane deformation measurements, and theoretical predictions show good agreement (within 15%). At 10-V actuation, the angular change is estimated at 486 μrad for this device. The uncertainty is largely limited to uncertainty in the membrane tilt when actuated.

5. Conclusion and Future Research

We have designed, fabricated, and demonstrated a piezoelectric-actuated analog tunable grating by me-

chanical deformation of a supporting submicrometer membrane. The design permits fine resolution below a nanometer for the grating period change, a tunable range up to several nanometers (corresponding to up to ~400 μrad), and minimizes out-of-plane motion of the membrane. Device fabrication utilizes both bulk and surface micromachining to improve device yield. The fabricated piezoelectric film shows an excellent dielectric constant of 1200. Mechanical measurements of the actuated device show grating period changes of 8.3 nm at 9 V and 4.9 nm at 10 V for two different device designs. For each device presented, the results agree well with our analytical and finite-element models. A diffraction angular change up to 486 μrad is measured at 10-V actuation, when corrected for membrane tilt in the matched finite-element modeling. Future design iterations will reduce the asymmetrical rotation, tilt, and bending of the membrane to improve the resolution in grating period change. Control of residual stress in a silicon nitride diffusion barrier would reduce bow in the membrane. To further reduce membrane bending, the membrane thickness could be increased for a cubic increase in bending stiffness, but the trade-off is a linear decrease in axial stiffness in the small-deflection regime.

The authors thank Salil Desai, Arnab Sinha, Kurt Broderick, Weiguo Liu, Dennis Freeman, and Martin Schmidt for their invaluable assistance. We appreciate the helpful discussions with Wei-Chuan Shih, Gregory Nielson, and Carlos Hidrovo, in addition to constructive criticism from two anonymous reviewers. This project was funded by ASML Holding N. V. Corporation.

References

1. R. B. Apte, F. Sandejas, W. Banyai, and D. Bloom, "Grating light valves for high resolution displays," in *Technical Digest of the Solid-State Sensors and Actuators Workshop* (Transducers Research Foundation, Cleveland Heights, Ohio, 1994), pp. 1–6.
2. G. B. Hocker, D. Youngner, E. Deutsch, A. Volpicelli, S. Senturia, M. Butler, M. Sinclair, T. Plowman, and A. J. Ricco, "The polychromator: a programmable MEMS diffraction grating for synthetic spectra," in *Technical Digest of the Solid-State Sensors and Actuators Workshop* (Transducers Research Foundation, Cleveland Heights, Ohio, 2000), pp. 89–92.
3. D. P. Resler, D. S. Hobbs, R. C. Sharp, L. J. Friedman, and T. A. Dorschner, "High-efficiency liquid-crystal optical phased-array beam steering," Opt. Lett. **21,** 689–691 (1996).
4. D. E. Sene, J. W. Grantham, V. M. Bright, and J. H. Comtois, "Development and characterization of micro-mechanical gratings for optical modulation," in *Proceedings of the ninth Annual International IEEE Micro Electro Mechanical Systems Workshop* (Institute of Electrical and Electronics Engineers, Piscataway, N.J., 1996), pp. 222–227.
5. X. M. Zhang and A. Q. Liu, "A MEMS pitch-tunable grating add/drop multiplexers," in *Proceedings of Optical MEMS* 2000 *IEEE/LEOS International Conference* (Institute of Electrical and Electronics Engineers, Piscataway, N.J., 2000), pp. 25–26.
6. T. Storgaard-Larsen, O. Leistiko, and S. Bouwstra, "Optomechanical accelerometer based on strain sensing by a Bragg grating in a planar waveguide," Sens. Actuators A **52,** 25–32 (1996).
7. B. E. A. Saleh and M. C. Teich, *Fundamentals of Photonics* (Wiley-Interscience, New York, 1991), pp. 799–831.
8. D. M. Burns and V. M. Bright, "Micro-electro-mechanical variable blaze gratings," in *Proceedings of IEEE MEMS Workshop* (Institute of Electrical and Electronics Engineers, Piscataway, N.J., 1997), pp. 55–60.
9. J. Castracane, M. A. Gutin, and O. N. Gutin, "Micromechanically controlled diffraction: a new tool for spectroscopy," in *Diffractive/Holographic Technologies and Spatial Light Modulators VII,* I. Cindrich, S. H. Lee, and R. L. Sutherland, eds., Proc. SPIE **3951,** 36–45 (2000).
10. W.-C. Shih, C. W. Wong, Y. B. Jeon, S.-G. Kim, and G. Barbastathis, "Electrostatic and piezoelectric analog tunable diffractive gratings," in *Conference on Lasers and Electro-Optics/Quantum Electronics and Lasers Science Conference,* Vol. 73 of 2002 OSA Trends in Optics and Photonics (Optical Society of America, Washington D.C., 2002), paper CMP4.
11. M. S. Weinberg, "Working equations for piezoelectric actuators and sensors," J. Microelectromech. Syst. **8,** 529–533 (1999).
12. S. D. Senturia, *Microsystem Design* in (Kluwer Academic, Boston, Mass. 2001), pp. 219–222.
13. S.-G. Kim and K.-H. Hwang, "Thin-film micromirror array (TMA) for large information display systems," J. Soc. Inf. Disp. **8,** 177–181 (2000).
14. W. Liu, J. S. Ko, and W. Zhu, "Preparation and properties of multiplayer Pb(Zr,Ti)O3/PbTiO3 thin films for pyroelectric application," Thin Solid Films **371,** 254–258 (2000).
15. D. M. Freeman, A. J. Aranyosi, M. J. Gordon, and S. S. Hong, "Multidimensional motion analysis of MEMS using computer microvision," in *Technical Digest of the Solid- State Sensors and Actuators Workshop* (Transducers Research Foundation, Cleveland Heights, Ohio, 1998), pp. 150–155.